Journal of Steroid Biochemistry and Molecular Biology 189 (2019) 19–27

Contents lists available at ScienceDirect

Journal of Steroid Biochemistry and Molecular Biology

journal homepage: www.elsevier.com/locate/jsbmb

Shedding light on the effects of 1,25-dihydroxyvitamin D_3 on epidermal lipid barrier formation in three-dimensional human skin equivalents

Arnout Mieremet[a,b], Rianne van Dijk[b], Gert Gooris[b], Joke A. Bouwstra[b,1], Abdoelwaheb El Ghalbzouri[a,1,*]

[a] Department of Dermatology, Leiden University Medical Centre, the Netherlands
[b] Division of BioTherapeutics, Leiden Academic Centre for Drug Research, the Netherlands

ARTICLE INFO

Keywords:
Primary cell culture
Artificial skin
Vitamin D
Calcitriol
Lipids
Ceramides
Tissue engineering

ABSTRACT

Human skin equivalents (HSEs) are three dimensional models resembling native human skin (NHS) in many aspects. Despite the manifold similarities to NHS, a restriction in its applications is the altered *in vitro* lipid barrier formation, which compromises the barrier functionality. This could be induced by suboptimal cell culturing conditions, which amongst others is the diminished activation of the vitamin D receptor (VDR) signalling pathway. The active metabolite of this signalling pathway is 1,25-dihydroxyvitamin D_3 ($1,25(OH)_2D_3$). An interacting role in the formation of the skin barrier has been ascribed to this pathway, although it remains unresolved to which extent this pathway contributes to the (mal-)formation of the epidermal barrier in HSEs. Our aim is to study whether cell culture medium enriched with $1,25(OH)_2D_3$ affects epidermal morphogenesis and lipid barrier formation in HSEs. Addition of 20 nM $1,25(OH)_2D_3$ resulted in activation of the VDR signalling pathway by inducing transcription of VDR target genes (CYP24A and LL37) in keratinocyte monocultures and in HSEs. Characterization of HSEs supplemented with $1,25(OH)_2D_3$ using immunohistochemical analyses revealed a high similarity in epidermal morphogenesis and in expression of lipid processing enzymes. The barrier formation was assessed using state-of-the art techniques analysing lipid composition and organization. Addition of $1,25(OH)_2D_3$ did not alter the composition of ceramides. Additionally, the lateral and lamellar organization of the lipids was similar, irrespective of supplementation. In conclusion, epidermal morphogenesis and barrier formation in HSEs generated in presence or absence of $1,25(OH)_2D_3$ leads to a similar morphogenesis and comparable barrier formation *in vitro*.

1. Introduction

The native human skin (NHS) is the largest organ of the body with the principle function to protect the body's interior from the external environment. Multiple defence mechanisms are formed to exert various functions of the skin including the physical, chemical, immunological, and microbial barrier [1]. Where possible, these are regulated to maintain local homeostasis, which is mediated by interactions of the cutaneous endocrine and neuroendocrine systems [2]. These are also integrated into central regulators by a continuous exchange of endocrine and neuroendocrine mediators between skin and other organs to preserve systemic homeostasis when adaptation to external stimuli is required [2]. The skin is directly exposed to ultraviolet (UV) radiation, acting as stressor for tissue homeostasis thereby inducing elements of the stress response [3]. Importantly, UV exposure is also driving the activation of vitamin D pathway in the skin. The active metabolite of the vitamin D pathway is 1α,25-dihydroxyvitamin D_3 ($1,25(OH)_2D_3$), which can bind to the vitamin D receptor (VDR). Upon activation, heterodimerization of VDR and retinoid-X receptor occurs, followed by binding to vitamin D response elements (VDREs) resulting

Abbreviations: NHS, native human skin; UV, ultraviolet; $1,25(OH)_2D_3$, 1α,25-dihydroxyvitamin D3; VDR, vitamin D receptor; VDREs, vitamin D response elements; SC, stratum corneum; FFAs, free fatty acids; ELOVLs, elongation of very long fatty acids; HSE, human skin equivalent; UGCG, ceramide glucosyltransferase; FTMs, full thickness models; FFPE, formalin fixed paraffin embedded; N.C., negative control; HE, haematoxylin and eosin; CYP24A, cytochrome P450 family 24 subfamily A; K, keratin; SCD1, stearoyl-CoA desaturase 1; $CERs_{total}$, total ceramide subclasses; CERs, ceramides of subclasses N and A; CER EO, ceramides of subclasses EO; LC–MS, liquid chromatography coupled to mass spectrometry; Glc-CER, glucosylceramide; AUC, area under curve; ISTD, internal standard; LPP, long periodicity phase; SPP, short periodicity phase; SAXD, small angle X-ray diffraction; FTIR, Fourier transform infrared spectroscopy

* Corresponding author at: Room C3-76, Albinusdreef 2, 2333 ZA, Leiden, the Netherlands.
E-mail address: a.ghalbzouri@lumc.nl (A. El Ghalbzouri).
[1] Senior authors contributed equally to this work.

https://doi.org/10.1016/j.jsbmb.2019.01.022
Received 12 December 2018; Received in revised form 17 January 2019; Accepted 30 January 2019
Available online 31 January 2019

in transcription of VDR target genes. These genes are involved in cellular proliferation, differentiation, and barrier formation of the skin [4–7]. The skin represents an autonomous vitamin D system due to the local synthesis of ligand $1,25(OH)_2D_3$ as well as expression of VDR in the various cell types of the skin [8].

The main physical barrier of the human skin resides in the uppermost layer of the epidermis. The stratum corneum (SC) consists of corneocytes embedded in a lipid matrix. Corneocytes are terminally differentiated keratinocytes, containing a thick cornified envelope [9–13]. Due to the cross-linked proteins, corneocytes are regarded to be impermeable for most substances. Consequently, diffusion of topical applied molecules mainly occurs through the intercorneocyte lipid matrix [14,15]. This matrix is connected to the corneocytes by the cornified lipid envelope. In the intercorneocyte space, the lipids are highly structured in the lateral and the lamellar organization [16]. The type of lipid organization influences the rate of compound penetration [17–19]. The main lipid classes in the SC lipid matrix are ceramides, free fatty acids (FFAs), and cholesterol [20]. The diversity in lipid composition is a result of numerous biosynthesis steps occurring in the epidermis. Various lipid processing enzymes or enzyme families are involved herein, as reviewed elsewhere [15,21–24]. Specifically, the diversity in carbon chain length is a result of regulated enzymatic lipid processing by the elongation of very long fatty acids (ELOVL) family.

The NHS is recapitulated *in vitro* by human skin equivalents (HSEs), which are the most sophisticated three-dimensional (3D) model systems. These exhibit the stratum basale, stratum spinosum, stratum granulosum and SC [25,26]. Consequently, HSEs form a physiological relevant *in vitro* model and are therefore widely applied in *in vitro* screenings of therapeutics and in toxicology assessments [27]. However, HSEs show dissimilar barrier properties as compared to NHS, potentially leading to altered *in vitro* - *in vivo* correlations or misclassifications of toxicology profiles [1,26]. Differences in composition and organization of the lipid matrix in the SC of HSEs as compared to NHS include but are not limited to the i) altered ceramide subclass profile, ii) reduced carbon chain length of FFAs and ceramides, iii) higher level of unsaturated lipids, iv) reduced repeat distance of lamellar phases, and v) increase in hexagonal lateral packing at the expense of the orthorhombic lateral packing [26,28]. Contributing factors to the aberrant barrier formation could be suboptimal culture medium composition or external culture conditions which are different from *in vivo*. HSEs are generated without exposure to sunlight or nutritional supplementation of $1,25(OH)_2D_3$, waning the activation of the vitamin D signalling pathway, which is in contrast to *in vivo* conditions.

A supporting role in the formation of the skin barrier has been ascribed to the vitamin D signalling pathway. The several roles that vitamin D plays during proliferation and differentiation of the keratinocytes in the epidermis is mediated by various coregulators [29,30]. Basically, $1,25(OH)_2D_3$ reduces cell proliferation, and promotes differentiation and cornified envelope formation [31]. Moreover, $1,25(OH)_2D_3$ is suggested to modulate the formation of the lipid barrier, mediated by altered expression of lipid processing enzymes ELOVL3, 4 and ceramide glucosyltransferase (UGCG) [4]. The interplay between the vitamin D signalling pathway and calcium signalling pathway regarding promotion of differentiation is captivating, as both induce differentiation, although these effects do not always seem to be in synergy [31,32]. Until today, it is unknown whether the vitamin D signalling pathway can contribute to normalization of cell proliferation, differentiation, and formation of the lipid barrier in 3D HSEs. Furthermore, to which extent the lack of $1,25(OH)_2D_3$ and/or sunlight exposure contributes to a compromised epidermal barrier in HSEs remains unresolved [26].

In this study, we aim to determine whether *in vitro* activation of the vitamin D signalling pathway affects epidermal morphogenesis and lipid barrier formation in HSEs. Addition of $1,25(OH)_2D_3$ in the cell culture medium during the generation of HSEs and subsequent analyses of the lipid barrier formation provides additional insights in the development of HSEs and formation of its barrier.

2. Materials and methods

2.1. Primary cell isolation and generation of skin models

Isolation of primary cells from the dermis and epidermis and cell culturing was performed as described before [33–35]. Full thickness models (FTMs) were generated as described before in a Memmert INC153med CO_2 incubator (Memmert, Schwabach, Germany) (Supplementary Fig. 1) [35]. The supplementation with 20 nM $1\alpha,25(OH)_2D_3$ (Sigma-Aldrich) or ethanol vehicle occurred twice a week for four times in total using serum-free high calcium medium (DMEM 3:1 (v/v) mixed with Ham's F12 (Gibco)), supplemented as described before [36]. Four different batches of FTMs were developed using unique primary cells and 3D models were generated for a total of 14 days at the air-liquid interface. Keratinocyte monocultures of three biological replicates were developed in 6-wells plates, in which 100.000 cells were plated per well. Cells reached 80% confluence in 3 days in low calcium medium (Dermalife medium (Lifeline Cell Technology) enriched with penicillin (10,000 U) and streptomycin (10 mg/ml). Subsequently, the medium was supplemented with 20 nM $1,25(OH)_2D_3$ or ethanol vehicle for 24 h. For high calcium medium condition, after reaching 80% confluence the keratinocytes were pre-incubated 24 h in serum high calcium medium (DMEM mixed 3:1 (v/v) with Ham's F12 supplemented with 5% fetal bovine serum (Hyclone, Logan, UT, USA)) and additives as described before [36]) to induce differentiation. Afterwards, supplementation for 24 h with $1,25(OH)_2D_3$ in high calcium medium occurred. Culture medium of all isolated primary cells was tested for mycoplasma contamination by qPCR and found negative.

2.2. Tissue imaging

Parts of NHS or FTM were 4% formaldehyde fixated and embedded in paraffin or snap frozen in liquid nitrogen. Haematoxylin and eosin (HE) staining was performed according to manufacturer's instructions (Klinipath, Duiven, The Netherlands). Protein analyses by immunohistochemistry or immunofluorescence were performed on 5 µm sections of both formalin fixed paraffin embedded (FFPE) or snap frozen material, as described earlier [35]. Specifications of the primary and secondary antibodies are provided in Supplementary Table 1. Estimations of the thickness of the viable epidermis was performed on four different regions per sample using Adobe Photoshop measuring the circumference of the viable epidermis. The amount of corneocyte layers was determined by safranin red staining and potassium hydroxide expansion of the SC following methods described earlier [37,38].

2.3. Gene expression

Total RNA was extracted from monocultures or from the viable epidermis of FTMs using the FavorPrep Tissue Total RNA Mini Kit (Favorgen, Ping-Tung, Taiwan) according to manufacturer's instruction. A DNA digestion step was added on-column using RNAse-free DNAse set (Qiagen, Hilden, Germany) for 15 min. Nucleic acid concentration was determined using a NanoDrop™ UV–vis Spectrophotometer (ThermoFisher). Complementary DNA was synthesized using 500 ng total RNA using the iScript™ cDNA Synthesis Kit (Bio-Rad, Hercules, USA) according to manufacturer's instructions. Quantitative real-time polymerase chain reaction was performed using the SYBR Green Supermix (Bio-Rad) on the CFX384™ real-time PCR detection system (Bio-Rad). Following settings were used: polymerase activation for 5 min at 95 °C, denaturation for 20 s at 95 °C, annealing for 20 s at 60 °C and extension for 20 s at 72 °C for 40 cycles followed by the generation of a melt curve. Data was normalized against the 2–3 most stable reference genes using the delta delta Ct method. Primers sequences are listed in Supplementary Table 2.

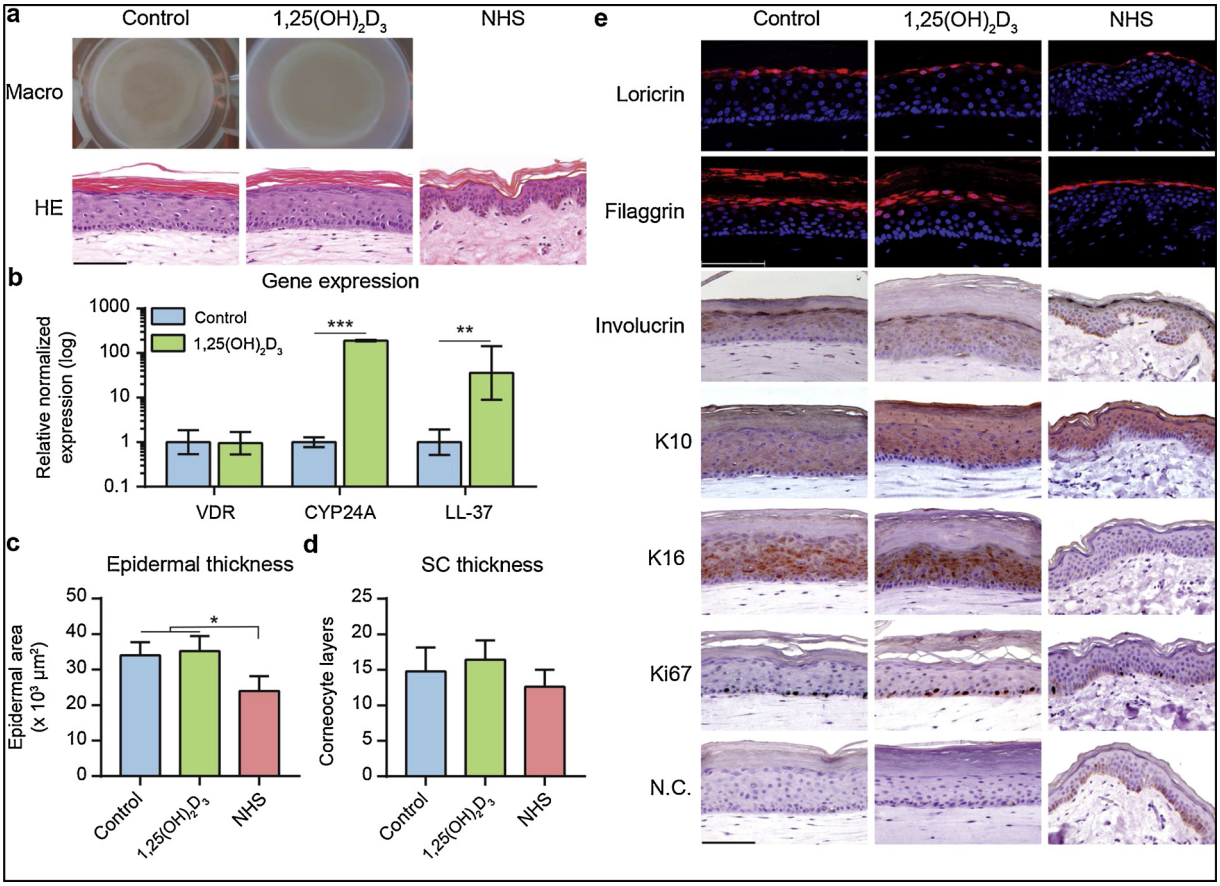

Fig. 1. General morphology of full thickness models after addition of 20 nM $1,25(OH)_2D_3$.
(a) Assessment of macro- and microanatomy, the latter after haematoxylin and eosin (HE) staining. **(b)** Epidermal gene expression of vitamin D receptor (VDR) and its target genes (CYP24 A and LL-37) in FTM-control and FTM-$1,25(OH)_2D_3$. Data indicates mean ± SD, N = 3. **(c)** Epidermal thickness of FTMs and of NHS. Data indicates mean + SD, N = 4. **(d)** Stratum corneum thickness of FTMs and of NHS, determined after safranin red staining and alkali expansion. Data indicates mean + SD, N = 4. **(e)** Expression of loricrin, filaggrin, involucrin, keratin 10 (K10), keratin 16 (K16), and Ki67 indicating epidermal differentiation programs, activation, and proliferation respectively. No non-specific binding of the secondary antibody was detected (negative control (N.C.)). Protein biomarkers are shown in red and nuclei in blue, scale bars indicate 100 µm.

2.4. Stratum corneum isolation and small angle X-ray diffraction analysis

SC was isolated after trypsin digestion, air-dried and stored under Argon gas over silica until further use as described before [35]. Small-angle X-ray diffraction (SAXD) measurements were performed at the European synchrotron radiation facility (Grenoble, France) at station BM26B for a period of 2 × 150 s as described elsewhere [18]. The scattering intensity I was measured as a function of the scattering vector q. The latter is defined as $q = \frac{4 \cdot \pi \cdot \sin\theta}{\lambda}$, in which θ is the scattering angle and λ is the wavelength. From the positions of the peaks (qn), the repeat distance can be calculated using the equation $d = \frac{2n \cdot \pi}{qn}$, where n is the order of diffraction peak [39].

2.5. Fourier transform infrared spectroscopy

The isolated SC was placed between two AgBr cells and put under continuous dry air for 30 min before the start of measurements. All spectra were acquired on a Varian 670-IR spectrometer equipped with a broad-band mercury cadmium telluride detector. The spectrometer was cooled with liquid nitrogen and connected to a controlled heating device. The spectrometer collected the data with a frequency range of 400-4000 cm^{-1}. The spectral resolution was 1 cm^{-1}. The measurements were performed with a 240 s time resolution. The lateral packing behaviour was examined between 0 °C and 40 °C with a heating rate of 0.25 °C/min, resulting in a 1 °C temperature increase per measurement. The software used to obtain and analyse spectra was Varian Resolutions Pro 5.2.0. Spectra were deconvoluted and finally processed with XRAY Plot program.

2.6. Liquid chromatography coupled to mass spectrometry analysis

Extraction of total lipids from isolated SC of FTMs was performed with an adjusted Bligh and Dyer method as described by Boiten et al. [40]. To determine the weight percentage of lipids in the SC, dry SC weight was measured before and after extraction. The lipids were analysed using normal phase liquid chromatography - mass spectrometry (LC–MS) according to the method described by Boiten et al. [40], with exception of the quantification to molar amounts. A total of 1500 ng lipids were separated on a PVA-Sil column (5 µM particles, 100 × 2.1 mm i.d.) (YMC, Kyoto, Japan) using an Acquity UPLC H-class (Waters, Milford, MA, USA) and detection occurred by a XEVO TQ-S mass spectrometer (Waters, Milford, MA, USA). Measurements were performed in full scan mode from 1.25 to 8.00 minutes between *m/z* 350–1350 for ceramides and from 8.0 to 12.5 minutes between *m/z* 500–1350 for glucosylceramides. Area under curve (AUC) were determined and corrected by ceramide N(24deuterated)S(18) as internal standard (ISTD).

2.7. Statistics

Statistical analyses are conducted using GraphPad Prism version 7.00 for Windows (GraphPad Software, La Jolla California USA).

Statistical testing was performed with 1-way or 2-way ANOVA with Tukey's post-test, otherwise specifically stated. Statistical differences are noted as *, ** or ***, corresponding to $P < 0.05$, < 0.01, < 0.001.

3. Results

3.1. Morphogenesis of HSEs supplemented with 1,25(OH)$_2$D$_3$

To determine the effect of vitamin D signalling pathway activation on epidermal morphogenesis and barrier formation, full thickness models (FTMs) were generated with cell culture medium which was enriched with 1α,25-dihydroxyvitamin D_3 (FTM-1,25(OH)$_2$D$_3$) or vehicle (FTM-control). Macroscopic examination revealed similarities in pigmentation, shape, and structure of FTMs in both conditions (Fig. 1**a**). Examination by haematoxylin and eosin (HE) showed the presence of all four epidermal layers in FTMs similar to NHS (Fig. 1**a**), indicating that supplementation with 1,25(OH)$_2$D$_3$ leads to a similar epidermal organization. The effects of 1,25(OH)$_2$D$_3$ supplementation was evaluated for the expression of VDR and of selected VDR target genes (LL-37 and CYP24A). Similar gene expression of VDR was observed after supplementation with 1,25(OH)$_2$D$_3$, whereas expression of both target genes was upregulated (Fig. 1**b**). This demonstrated that the delivery of 1,25(OH)$_2$D$_3$ was successful to the epidermis of the FTMs, despite its poor solubility and presence of albumin in the culture medium. In addition, the vast fold change indicated that the utilized concentration was adequate. To further assess epidermal characteristics, the thickness of the viable epidermis was quantified and compared (Fig. 1**c**). This revealed that supplementation with 1,25(OH)$_2$D$_3$ did not alter epidermal thickness, whereas the epidermis of NHS was significantly thinner as compared to FTMs. The number of corneocyte layers in the SC was equal in all conditions and comparable to NHS **(**Fig. 1**d**). The epidermal morphogenesis was further studied using expression of specific morphogenesis biomarkers for epidermal differentiation, cell activation and basal layer proliferation (Fig. 1**e**). For validation, the expression of these biomarkers was also studied in NHS. From apical to basal side, examination of late (loricrin, filaggrin and involucrin) and early epidermal differentiation (keratin (K)10) revealed no effect of activated vitamin D signalling pathway on the execution of the differentiation programs. Comparison with the differentiation programs in NHS revealed a similar early, but distinct late epidermal differentiation program, as the granular layer in FTMs was enlarged and expression of involucrin initiated in the spinous layer. The equal expression of biomarker K16 indicated an activated state of FTMs, instead of no K16 expression and full homeostasis observed in NHS. The expression of Ki67 positive cells in the basal layer (proliferation) was similar irrespective the conditions tested. The proliferation indexes were: FTM-control (17.7 ± 3.9), FTM-1,25(OH)$_2$D$_3$ (20.6 ± 8.7), and NHS (12.1 ± 0.4).

3.2. Lipid processing after supplementation with 1,25(OH)$_2$D$_3$

The expression of lipid processing enzymes which play an important role in the barrier formation was evaluated on protein level in FTM-control, FTM-1,25(OH)$_2$D$_3$, and NHS (Fig. 2**a**). Similar expression of ELOVL family members 1, 3, 4, and 6 was detected, irrespective of supplementation with 1,25(OH)$_2$D$_3$. Protein expression of stearoyl-CoA desaturase-1 (SCD1) was detected comparably in both FTMs. As compared to NHS, an increased expression of ELOVL1 and SCD1 was detected in FTMs. Additionally, expression of these lipid processing enzymes was also assessed in UV light (UVA and UVB) irradiated FTMs, which compensates for the diminished sunlight exposure in another way than supplementation with 1,25(OH)$_2$D$_3$ does (Supplementary Fig. 2). Evaluation of the expression of lipid processing enzymes in these FTMs showed a similar expression profile as non-irradiated FTMs. However, high dose UV (≥ 90 mJ/cm^2) exposure did lead to apoptosis, while in low dose UV (< 90 mJ/cm^2) irradiation this was undetected. In case of apoptosis, the lipid processing enzyme expression reduced, possibly linked to reduced viability.

To obtain more insights on the equal expression of lipid processing enzymes after 1,25(OH)$_2$D$_3$ supplementation, the contribution of extracellular calcium was determined in primary proliferating and differentiating keratinocyte monocultures. Examination of gene expression of VDR and its downstream targets revealed a similar expression of VDR and upregulated expression of CYP24B and LL-37, indicative for an effective delivery of 1,25(OH)$_2$D$_3$ (Fig. 2**b**). Expression of ELOVL family members 1, 4 and 6 was unchanged after 1,25(OH)$_2$D$_3$ supplementation (Fig. 2**c**). Solely an increased expression of ELOVL4 was detected due to the elevated external calcium levels. Furthermore, the protein barrier formation was promoted due to the calcium concentration indicated by elevated involucrin expression, but was similar regardless of supplementation with 1,25(OH)$_2$D$_3$ (Fig. 2**d**). These complementary findings indicate that the lipid processing is similar, irrespective of 1,25(OH)$_2$D$_3$ supplementation or UV light exposure.

3.3. Ceramide composition of the intercorneocyte lipid matrix

To obtain more insights on the epidermal barrier formation, the ceramide composition in the SC was studied. The total lipid content within the SC was similar in all conditions tested (Supplementary Fig. 3a). Although three main classes of lipids are present in the SC, the ceramides are very characteristic in the SC composition and are crucial for the lipid organization. Therefore, we focused on the twelve most abundant ceramide subclasses in the SC lipid matrix (Fig. 3**a**). After separation by polarity and detection per mass using the in-house developed liquid chromatography coupled to mass spectrometry (LC–MS) approach [40], the ceramide subclasses were analysed (Supplementary Fig. 3b). Comparisons were made for the profiles of the total ceramide subclasses ($CERs_{total}$) of FTM-control and FTM-1,25(OH)$_2$D$_3$, which showed a high similarity for ceramides of subclasses N and A (CERs) and for ceramides of subclasses EO (CER EO) in both conditions (Fig. 3**b, c**). The ceramide composition was examined in more detail by analysing the carbon chain length distribution. A wide distribution in the carbon chain length of the CERs was observed, from CERs with 32 carbon atoms to CERs with 54 carbon atoms (Fig. 3**d**). The broad distribution in carbon chain length was also detected for the CERs EO, ranging between 64 and 74 total carbon atoms (Fig. 3**e**). The carbon chain length distribution for all CERs and CERs EO was similar in both conditions tested. Next, the level of unsaturation in four CER subclasses was studied, serving as an indication for the degree of unsaturation in $CERs_{total}$ (Helder et al., in preparation). This revealed that the CERs in both FTMs have a similar percentage of monounsaturation (Supplementary Fig. 3c). In addition, the levels of glucosylceramides (Glc-CERs) were investigated, as these are important $CERs_{total}$ precursors. These showed a variability in their presence based on the two-dimensional ion plot (Supplementary Fig. 3d). Calculation of the glucosylceramide index revealed that 1,25(OH)$_2$D$_3$ supplementation did lead to reduction in the amount of Glc-CERs, showing a difference in the lipid precursors of the SC lipid matrix barrier formation after 1,25(OH)$_2$D$_3$ supplementation (Supplementary Fig. 3e).

3.4. Intercorneocyte lipid organization

Analysis of the barrier formation in FTM-control and FTM-1,25(OH)$_2$D$_3$ continued with assessment of the lipid organization in the SC (Fig. 4**a, b**). The lipid lamellae in the SC can be organized in either the short periodicity phase (SPP) or the long periodicity phase (LPP) (Fig. 4**c**). In the direction perpendicular to the lamellar stacking within the lipid matrix, the lipids are arranged in a lateral organization (Fig. 4**d**). In the orthorhombic lateral packing, the hydrocarbon chains of the lipids form the most dense packing. The hexagonal lateral packing is characterized by a less dense packing, enabling lipid rotation along their axis. SAXD was utilized to determine the repeat distance of

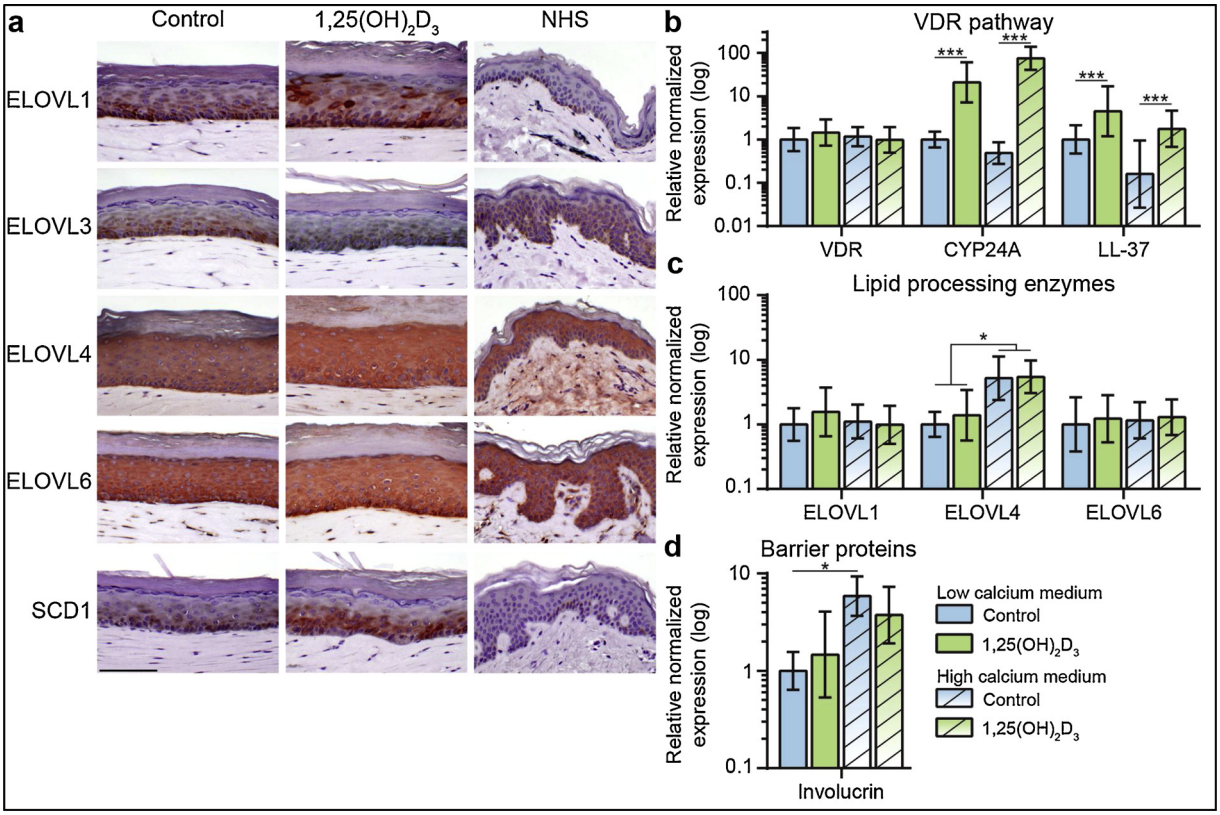

Fig. 2. Lipid processing enzyme expression after addition of 20 nM $1,25(OH)_2D_3$.
Representative images show the expression and localization of lipid processing enzyme which are involved in elongation (ELOVL1, 3, 4, 6) or desaturation (SCD1) of SC barrier lipids in FTMs and NHS. Enzymes are shown in red and nuclei in blue, scale bar indicates 100 µm. **(b–d)** Expression profiles of **(b)** genes involved in the VDR pathway, **(c)** lipid processing enzymes, and **(d)** skin barrier proteins in keratinocyte monocultures. Gene expression was determined after supplementation with $1,25(OH)_2D_3$ or vehicle in low or high calcium medium. Data represents mean ± SD, N = 3.

the lamellar phases (Fig. 4**e**). In the diffraction pattern of FTM-control and FTM-$1,25(OH)_2D_3$ a series of peaks were observed demonstrating the presence of the LPP with similar repeat distances, although this distance is shorter than that observed in NHS [39] (Fig. 4**g**). An additional phase was observed in the representative profiles, although inconsistently throughout the batches for both the FTM-control and FTM-$1,25(OH)_2D_3$, indicating no induction or aggravation of aberrant phase formation by $1,25(OH)_2D_3$. As compared to NHS, no diffraction peaks attributed to the SPP were observed. The lateral organization was examined using Fourier transform infrared spectroscopy (FTIR). Methylene rocking vibrations are detected which consists of two peaks at 720 cm^{-1} and 730 cm^{-1} when lipids adopt an orthorhombic packing, whereas only a single peak at 720 cm^{-1} is detected when lipids adopt a hexagonal packing (Fig. 3**f**). The predominant hexagonal lateral packing was observed in all FTMs, irrespective supplementation with $1,25(OH)_2D_3$ (Fig. 3**h**). In NHS, the lipids were arranged predominantly in the orthorhombic lateral organization, which remained present even at 40 °C.

4. Discussion

In this study, we aimed to unravel the effects of $1,25(OH)_2D_3$ on epidermal morphogenesis and lipid barrier formation during *in vitro* development of human skin equivalents. In the present report, we showed that addition of $1,25(OH)_2D_3$ in the cell culture medium activated the vitamin D signalling pathway, although this did not affect epidermal morphogenesis in FTMs. Moreover, the lipid barrier formation remained comparable for the ceramide composition and lipid organization.

The similar proliferation rate and the unaltered expression of involucrin in FTM-$1,25(OH)_2D_3$ as compared to FTM-control are of specific interest. A similar proliferation rate was not observed in monocultures of keratinocytes [44]. However, anti-proliferative effects were reported in 2D keratinocyte cultures, whereas in this study 3D models with a supportive viable dermal equivalent were used. Furthermore, additional explanations on the diverge results on proliferation could be either the high calcium concentration in the FTM culture medium (± 1.43 mM) [45] or the occurrence of $1,25(OH)_2D_3$ catabolism over time mediated by increased CYP24A gene expression [46,47]. The expression of the structural protein involucrin, with a VDRE in the promoter region, was shown to be upregulated after $1,25(OH)_2D_3$ supplementation before in monocultures of keratinocytes [48,49]. Our keratinocyte monocultures showed upregulated involucrin gene expression after high calcium treatment, but no additional effect was observed after $1,25(OH)_2D_3$ supplementation. Furthermore, no altered involucrin protein expression was detected in FTM-$1,25(OH)_2D_3$ as compared to FTM-control. This partial discrepancy to literature could be explained by lack of synergic effects of high calcium and $1,25(OH)_2D_3$ supplementation during longer incubation periods, as reported before [48,50,51]. Besides, involucrin is expressed in FTMs in the stratum granulosum and stratum spinosum, which contrasts with the restricted expression in the stratum granulosum in NHS, contributing to high level of complexity interpreting the result for this protein. Other interactions between calcium and vitamin D signalling pathways are discussed elsewhere [32,52]. Based on these interactions and similar effects, the calcium pathway is suggested as the major factor minimizing the effectiveness of $1,25(OH)_2D_3$ supplementation in 3D models. Alternatively, activation of distinct signalling transduction pathways by $1,25(OH)_2D_3$ involving other nuclear receptors expressed by keratinocytes and fibroblasts could occur [53,54]. Additionally, the

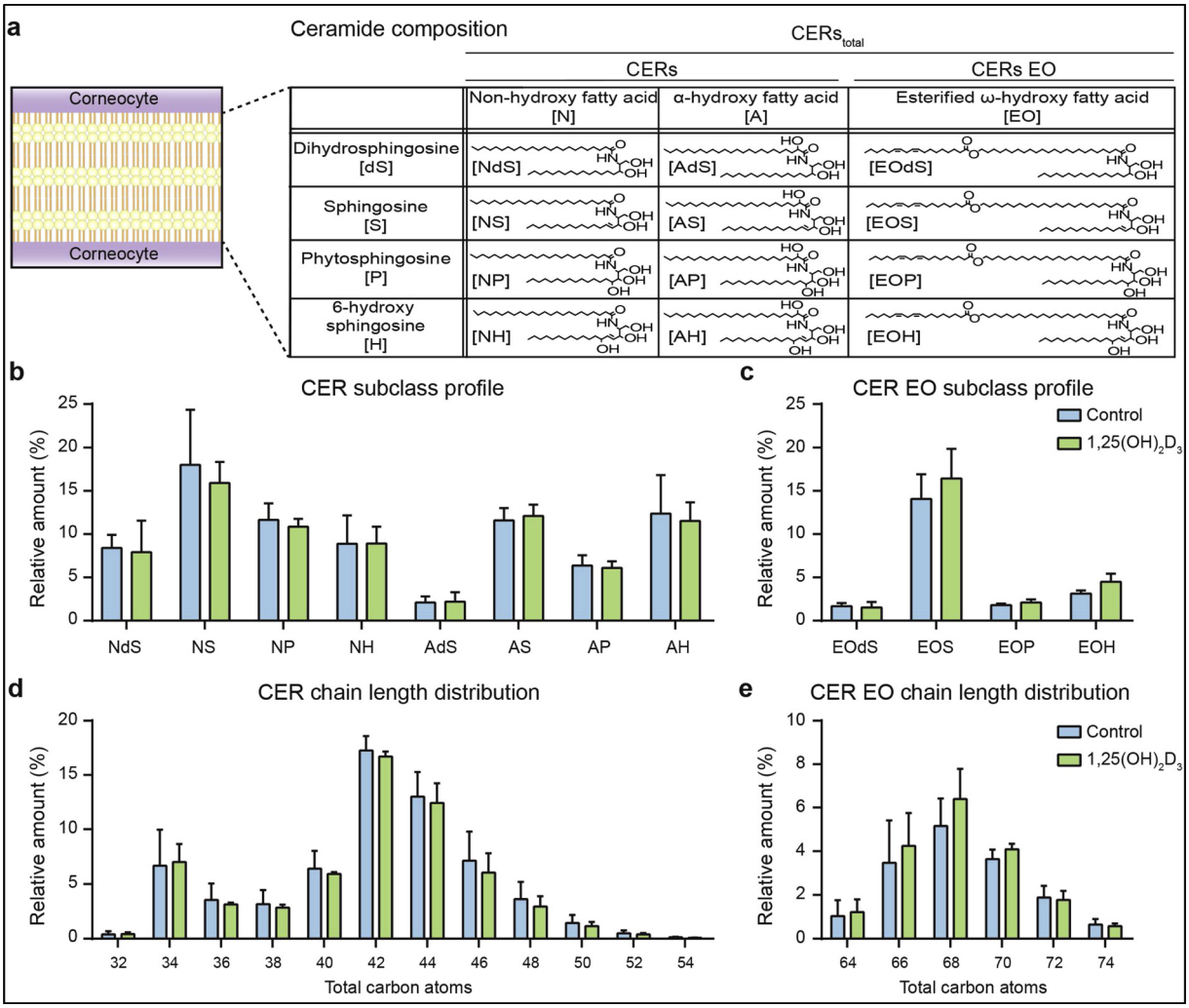

Fig. 3. Ceramide composition in the lipid matrix of the stratum corneum in FTM-control and FTM-1,25$(OH)_2D_3$.
(a) Schematic overview of the lipids in the intercorneocyte space. Tabular overview provides structural formulas of the twelve most abundant ceramide subclasses with nomenclature according to Motta et al. [41]. **(b)** Bar plot showing CER subclass profiles. **(c)** Bar plot showing CER EO subclass profiles. Subclass profiles are shown in relative abundance as percentage of total AUC/ISTD of $CERs_{total}$. **(d)** Bar plot of CER carbon chain length distributions. **(e)** Bar plot of CER EO carbon chain length distributions. Carbon chain length distributions are presented in relative abundance as percentage of total AUC/ISTD of $CERs_{total}$. A concentration of 20 nM 1,25$(OH)_2D_3$ was added. All data indicates mean + SD, N = 4.

activation of vitamin D by alternative pathways forming structurally different but potent metabolites have been suggested [55–57]. Phenotypic characteristics of proliferation and differentiation are often difficult to link to a single signalling pathway or metabolite due to the myriad overlapping and intercommunication pathways. Further preclinical studies using a phenotypic relevant model need to be performed to disentangle this.

The barrier formation was studied before by Oda et al. [4] in submerged monocultures of keratinocytes, in which the ELOVL3, ELOVL4, and UGCG expression and/or activity was altered after VDR or VDR coactivator knockdown. However, supportive effects on ELOVL expression were not observed in this study after activation of VDR signalling pathway or UV exposure in 3D HSEs. The comparable epidermal location of ELOVL 3, 4 and 6 proteins was observed in HSEs, irrespective of supplementation. Furthermore, the equal ceramide chain length distribution profiles of FTM-1,25$(OH)_2D_3$ and FTM-control supports similar ELOVL functionality after VDR activation *in vitro*. As compared to NHS, ELOVL1 is more expressed in HSEs. This is ascribed to its role in elongation of unsaturated lipids, which are more present in HSEs and are associated with the elevated expression of SCD1 [21].

The reduced presence of Glc-CERs in the SC of FTM-1,25$(OH)_2D_3$ is linked to the modified Glc-CER content observed after VDR knockdown [4]. This suggests an important role of VDR in the regulation of Glc-CER formation and adds another layer of significance on the interplay between 1,25$(OH)_2D_3$ and the epidermal barrier formation. However, the barrier lipid organization remained equal in both conditions, in line with the similar $CERs_{total}$ composition. A limitation of the ceramide composition analysis is the lack of quantification of the LC–MS data, due to a high technical complexity in the data analysis, concomitant with analysis of the various CERs EO esterified entities (Helder et al., in preparation). This leads to underestimation of the abundance of CERs EO, although the interpretations and conclusions drawn from the data are not affected by this.

Recent observations reported the upregulation of the antimicrobial defence mechanism after vitamin D culture medium supplementation in HSEs [34]. Besides, there is accumulating evidence that the activation of the vitamin D signalling pathway influences the anti-inflammatory pathway [58,59], making the vitamin D signalling pathway of high interest regarding the immune barrier function of the skin. In this study, the increased expression of LL-37 as part of the antimicrobial defence mechanism was observed. Akiyama et al. [60] described that this peptide upregulates tight junction-related proteins and thereby

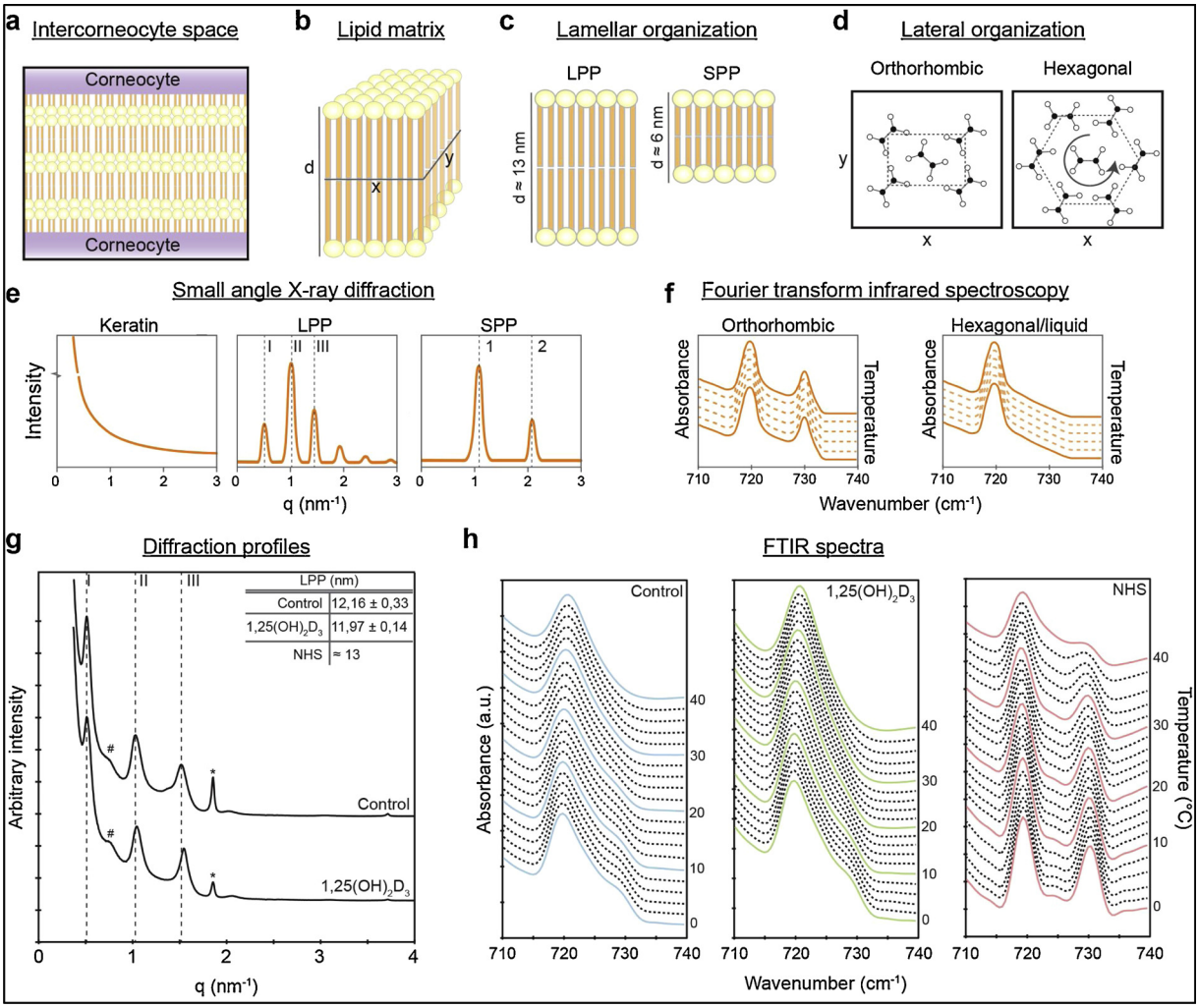

Fig. 4. Intercorneocyte lipid matrix organization.
(a) Schematic overview of the intercorneocyte space in the stratum corneum. **(b)** Three-dimensional schematic overview of the lipid matrix in the intercorneocyte space. Lipids are drawn in hairpin conformation, although lipids could also adapt the extended conformation [42,43]. **(c)** Schematic simplified overview of the lamellar organization of the lipid matrix. The long periodicity phase (LPP) has an approximate repetition distance (d) of 13 nm and the short periodicity phase (SPP) has an approximate d of 6 nm [39]. **(d)** Schematic presentation of hydrocarbon chains in the lateral organization. In the orthorhombic organization, lipids form the most dense packing. The hexagonal organization is characterized by a dense packing, with equal density in plane perpendicular to the hydrocarbon chains enabling lipids to rotate along their axis [16]. **(e)** Concepts of Small Angle X-ray Diffraction (SAXD) plots of isolated keratin, LPP and SPP. Diffraction profiles are generated by plotting the scattering intensity (arbitrary unit) as a function of the scattering vector q (in nm^{-1}). **(f)** Principles of Fourier Transform Infrared Spectroscopy (FTIR) profiles in the methylene rocking vibration spectrum. In the orthorhombic lateral packing, the spectrum in the rocking vibration region consists of two peaks located at 720 and 730 cm^{-1}. In contrast, in the hexagonal lateral packing the spectrum in the rocking vibration regions consist of one peak at 720 cm^{-1}. **(g)** SAXD profiles of FTM-control and of FTM-1,25$(OH)_2D_3$. Representative diffraction pattern in which the first, second and third diffraction order of the long periodicity phase (LPP) are indicated by the dotted line with Roman numbers (I, II, and III). Phase separated crystalline cholesterol is indicated by the asterisk (*), whereas phase separated lipids of unknown origin are indicated by the number sign (#). Inset provides tabular overview of repeat distances of the LPP, indicated for FTMs and for NHS by mean ± SD, N = 4 [39]. **(h)** Representative FTIR spectra of the methylene rocking vibrational mode of lipids. Spectra are shown for FTM-control, FTM-1,25$(OH)_2D_3$ and of NHS. In the rocking vibration region of the spectrum in both FTMs a single peak at 720 cm^{-1} was detected, whereas in NHS two peaks were detected. A concentration of 20 nM 1,25$(OH)_2D_3$ was added.

reinforces the epidermal barrier function on protein barrier level. Various studies reported the beneficial effect of 1,25$(OH)_2D_3$ supplementation of skin-resident immune cells, including dermal dendritic cells and Langerhans cells [59]. However, as the current FTMs are immune incompetent and do not contain vascular and nerve structures, the behaviour of these cell types and the link to systemic effects could not be studied. Notably, 1,25$(OH)_2D_3$ addition to in immune competent HSEs should therefore not be overlooked [61,62]. This could lead to higher preclinical relevance, as vitamin D and its analogues are used in the treatment of skin diseases [8]. However, we determined the effects of 1,25$(OH)_2D_3$ in co-culture of solely keratinocytes and fibroblasts, yielding novel insights in the barrier formation based on these cell types, thereby excluding effects based on immune cell (de-)activation.

In conclusion, the effect of vitamin D signalling pathway activation on the epidermal morphogenesis and barrier formation was characterized in detail based on the expression of morphogenesis biomarkers and lipid processing enzymes and extensive profiling of the lipid composition and organization. This revealed no major differences after addition of 1,25$(OH)_2D_3$ to the cell culture medium of FTMs, mainly ascribed to high calcium levels in the culture medium. These novel insights provide valuable information about the influence of culture medium and environmental factors on the barrier formation in HSEs, which are important in the reconstruction of skin models mimicking physiological or pathophysiological conditions.

Conflict of interest

The authors have declared no conflicting interests.

Acknowledgements

This research was financially supported by Dutch Technology Foundation STW (grant no. 13151), which is part of the Netherlands Organisation for Scientific Research (NWO), and is partly funded by the Dutch Ministry of Economic Affairs. The authors would like to thank the personnel at the DUBBLE beam line (BM26) at the European synchrotron radiation facility for their support with the SAXD measurements. Samira Absalah is thanked for her support with the lipid extraction and the liquid chromatography coupled to mass spectrometry run. Pieter Voskamp is thanked for his contribution with UV irradiation of HSEs. We thank the company Evonik (Essen, Germany) for their generous provision of CERs.

Appendix A. Supplementary data

Supplementary material related to this article can be found, in the online version, at doi:https://doi.org/10.1016/j.jsbmb.2019.01.022.

References

[1] H. Niehues, J.A. Bouwstra, A. El Ghalbzouri, J.M. Brandner, P.L.J.M. Zeeuwen, E.H. Bogaard, 3D skin models for 3R research: the potential of 3D reconstructed skin models to study skin barrier function, Exp. Dermatol. 27 (2018) 501–511, https://doi.org/10.1111/exd.13531.

[2] A.T. Slominski, M.A. Zmijewski, C. Skobowiat, B. Zbytek, R.M. Slominski, J.D. Steketee, Sensing the environment: regulation of local and global homeostasis by the skin's neuroendocrine system, Adv. Anat. Embryol. Cell Biol. 212 (2012) v-115, https://doi.org/10.1007/978-3-642-19683-6_1.

[3] A.T. Slominski, M.A. Zmijewski, P.M. Plonka, J.P. Szaflarski, R. Paus, How UV light touches the brain and endocrine system through skin, and why, Endocrinology 159 (2018) 1992–2007, https://doi.org/10.1210/en.2017-03230.

[4] Y. Oda, Y. Uchida, S. Moradian, D. Crumrine, P.M. Elias, D.D. Bikle, Vitamin D receptor and coactivators SRC2 and 3 regulate epidermis-specific sphingolipid production and permeability barrier formation, J. Invest. Dermatol. 129 (2009) 1367–1378, https://doi.org/10.1038/jid.2008.380.

[5] N. Hill, J. Zhang, M. Leonard, M. Lee, H. Shamma, M. Kadakia, 1α, 25-Dihydroxyvitamin D 3 and the vitamin D receptor regulates ΔNp63α levels and keratinocyte proliferation, Cell Death Dis. 6 (2015) e1781, https://doi.org/10.1038/cddis.2015.148.

[6] B. Lehmann, K. Querings, J. Reichrath, Vitamin D and skin: new aspects for dermatology, Exp. Dermatol. 13 (2004) 11–15, https://doi.org/10.1111/j.1600-0625.2004.00257.x.

[7] D.D. Bikle, Vitamin D and the skin: physiology and pathophysiology, Rev. Endocr. Metab. Disord. 13 (2012) 3–19, https://doi.org/10.1007/s11154-011-9194-0.

[8] J. Reichrath, C.C. Zouboulis, T. Vogt, M.F. Holick, Targeting the vitamin D endocrine system (VDES) for the management of inflammatory and malignant skin diseases: an historical view and outlook, Rev. Endocr. Metab. Disord. 17 (2016) 405–417, https://doi.org/10.1007/s11154-016-9353-4.

[9] E. Candi, R. Schmidt, G. Melino, The cornified envelope: a model of cell death in the skin, Nat. Rev. Mol. Cell Biol. 6 (2005) 328–340, https://doi.org/10.1038/nrm1619.

[10] B. Jackson, C.M. Tilli, M.J. Hardman, A.A. Avilion, M.C. MacLeod, G.S. Ashcroft, C. Byrne, Late cornified envelope family in differentiating epithelia—response to calcium and ultraviolet irradiation, J. Invest. Dermatol. 124 (2005) 1062–1070, https://doi.org/10.1111/j.0022-202X.2005.23699.x.

[11] J.M. Brandner, M. Haftek, C.M. Niessen, Adherens junctions, desmosomes and tight junctions in epidermal barrier function, Open Dermatol. J. 4 (2010) 14–20, https://doi.org/10.2174/1874372201004010014.

[12] M. Haftek, S. Callejon, Y. Sandjeu, K. Padois, F. Falson, F. Pirot, P. Portes, F. Demarne, V. Jannin, Compartmentalization of the human stratum corneum by persistent tight junction-like structures, Exp. Dermatol. 20 (2011) 617–621, https://doi.org/10.1111/j.1600-0625.2011.01315.x.

[13] M. Yokouchi, T. Atsugi, M. van Logtestijn, R.J. Tanaka, M. Kajimura, M. Suematsu, M. Furuse, M. Amagai, A. Kubo, Epidermal cell turnover across tight junctions based on Kelvin's tetrakaidecahedron cell shape, eLife 5 (2016) e19593, , https://doi.org/10.7554/eLife.19593.001.

[14] H. Trommer, R. Neubert, Overcoming the stratum corneum: the modulation of skin penetration, Skin Pharmacol. Physiol. 19 (2006) 106–121, https://doi.org/10.1159/000091978.

[15] J. Van Smeden, M. Janssens, G. Gooris, J. Bouwstra, The important role of stratum corneum lipids for the cutaneous barrier function, Biochim. Biophys. Acta (BBA)-Mol. Cell Biol. Lipids 1841 (2014) 295–313, https://doi.org/10.1016/j.bbalip.2013.11.006.

[16] M. Boncheva, F. Damien, V. Normand, Molecular organization of the lipid matrix in intact Stratum corneum using ATR-FTIR spectroscopy, Biochim. Biophys. Acta (BBA) – Biomembr. 1778 (2008) 1344–1355, https://doi.org/10.1016/j.bbamem.2008.01.022.

[17] D. Groen, D.S. Poole, G.S. Gooris, J.A. Bouwstra, Is an orthorhombic lateral packing and a proper lamellar organization important for the skin barrier function? Biochim. Biophys. Acta (BBA) – Biomembr. 1808 (2011) 1529–1537, https://doi.org/10.1016/j.bbamem.2010.10.015.

[18] E.H. Mojumdar, R.W. Helder, G.S. Gooris, J.A. Bouwstra, Monounsaturated fatty acids reduce the barrier of stratum corneum lipid membranes by enhancing the formation of a hexagonal lateral packing, Langmuir 30 (2014) 6534–6543, https://doi.org/10.1021/la500972w.

[19] F. Damien, M. Boncheva, The extent of orthorhombic lipid phases in the stratum corneum determines the barrier efficiency of human skin in vivo, J. Invest. Dermatol. 130 (2010) 611–614, https://doi.org/10.1038/jid.2009.272.

[20] P.W. Wertz, B. van den Bergh, The physical, chemical and functional properties of lipids in the skin and other biological barriers, Chem. Phys. Lipids 91 (1998) 85–96, https://doi.org/10.1016/S0009-3084(97)00108-4.

[21] A. Kihara, Synthesis and degradation pathways, functions, and pathology of ceramides and epidermal acylceramides, Prog. Lipid Res. 63 (2016) 50–69, https://doi.org/10.1016/j.plipres.2016.04.001.

[22] B. Breiden, K. Sandhoff, The role of sphingolipid metabolism in cutaneous permeability barrier formation, Biochim. Biophys. Acta 1841 (2014) 441–452, https://doi.org/10.1016/j.bbalip.2013.08.010.

[23] K.R. Feingold, P.M. Elias, Role of lipids in the formation and maintenance of the cutaneous permeability barrier, Biochim. Biophys. Acta 1841 (2014) 280–294, https://doi.org/10.1016/j.bbalip.2013.11.007.

[24] M. Rabionet, K. Gorgas, R. Sandhoff, Ceramide synthesis in the epidermis, Biochim. Biophys. Acta 1841 (2014) 422–434, https://doi.org/10.1016/j.bbalip.2013.08.011.

[25] A. El Ghalbzouri, P. Hensbergen, S. Gibbs, J. Kempenaar, R. van der Schors, M. Ponec, Fibroblasts facilitate re-epithelialization in wounded human skin equivalents, Lab. Investig. 84 (2004) 102–112, https://doi.org/10.1038/labinvest.3700014.

[26] V.S. Thakoersing, G.S. Gooris, A. Mulder, M. Rietveld, A. El Ghalbzouri, J.A. Bouwstra, Unraveling barrier properties of three different in-house human skin equivalents, Tissue Eng. Part C Methods 18 (2011) 1–11, https://doi.org/10.1089/ten.tec.2011.0175.

[27] S.H. Mathes, H. Ruffner, U. Graf-Hausner, The use of skin models in drug development, Adv. Drug Deliv. Rev. 69–70 (2014) 81–102, https://doi.org/10.1016/j.addr.2013.12.006.

[28] V.S. Thakoersing, J. van Smeden, A.A. Mulder, R.J. Vreeken, A. El Ghalbzouri, J.A. Bouwstra, Increased presence of monounsaturated fatty acids in the stratum corneum of human skin equivalents, J. Invest. Dermatol. 133 (2013) 59–67, https://doi.org/10.1038/jid.2012.262.

[29] Y. Oda, M.H. Ishikawa, N.P. Hawker, Q.C. Yun, D.D. Bikle, Differential role of two VDR coactivators, DRIP205 and SRC-3, in keratinocyte proliferation and differentiation, J. Steroid Biochem. Mol. Biol. 103 (2007) 776–780, https://doi.org/10.1016/j.jsbmb.2006.12.069.

[30] Y. Oda, C. Sihlbom, R.J. Chalkley, L. Huang, C. Rachez, C.P. Chang, A.L. Burlingame, L.P. Freedman, D.D. Bikle, Two distinct coactivators, DRIP/mediator and SRC/p160, are differentially involved in vitamin D receptor transactivation during keratinocyte differentiation, Mol. Endocrinol. (Baltimore, Md.) 17 (2003) 2329–2339, https://doi.org/10.1210/me.2003-0063.

[31] D.D. Bikle, S. Pillai, Vitamin D, calcium, and epidermal differentiation*, Endocr. Rev. 14 (1993) 3–19, https://doi.org/10.1210/edrv-14-1-3.

[32] D.D. Bikle, Vitamin D metabolism and function in the skin, Mol. Cell. Endocrinol. 347 (2011) 80–89, https://doi.org/10.1016/j.mce.2011.05.017.

[33] A. El Ghalbzouri, S. Commandeur, M.H. Rietveld, A.A. Mulder, R. Willemze, Replacement of animal-derived collagen matrix by human fibroblast-derived dermal matrix for human skin equivalent products, Biomaterials 30 (2009) 71–78, https://doi.org/10.1016/j.biomaterials.2008.09.002.

[34] E.M. Haisma, M.H. Rietveld, A. de Breij, J.T. van Dissel, A. El Ghalbzouri, P.H. Nibbering, Inflammatory and antimicrobial responses to methicillin-resistant *Staphylococcus aureus* in an *in vitro* wound infection model, PLoS One 8 (2013) e82800, , https://doi.org/10.1371/journal.pone.0082800.

[35] A. Mieremet, M. Rietveld, S. Absalah, J. van Smeden, J.A. Bouwstra, A. El Ghalbzouri, Improved epidermal barrier formation in human skin models by chitosan modulated dermal matrices, PLoS One 12 (2017) e0174478, , https://doi.org/10.1371/journal.pone.0174478.

[36] P. Voskamp, C.A. Bodmann, H.G. Rebel, G.E. Koehl, C.P. Tensen, J.N. Bouwes Bavinck, A. El Ghalbzouri, H.J. Van Kranen, R. Willemze, E.K. Geissler, F.R. De Gruijl, Rapamycin impairs UV induction of mutant-p53 overexpressing cell clusters without affecting tumor onset, Int. J. Cancer 131 (2012) 1267–1276, https://doi.org/10.1002/ijc.27391.

[37] A. Mieremet, M. Rietveld, R. van Dijk, J.A. Bouwstra, A. El Ghalbzouri, Recapitulation of native dermal tissue in a full-thickness human skin model using human collagens, Tissue Eng. Part A 24 (2018) 873–881, https://doi.org/10.1089/ten.TEA.2017.0326.

[38] S. Sakai, Y. Endo, N. Ozawa, T. Sugawara, A. Kusaka, T. Sayo, S. Inoue, H. Tagami, Characteristics of the epidermis and stratum corneum of hairless mice with experimentally induced diabetes mellitus, J. Invest. Dermatol. 120 (2003) 79–85, https://doi.org/10.1046/j.1523-1747.2003.12006.x.

[39] J.A. Bouwstra, G.S. Gooris, J.A. van der Spek, W. Bras, Structural investigations of human stratum corneum by small-angle X-ray scattering, J. Invest. Dermatol. 97 (1991) 1005–1012, https://doi.org/10.1111/1523-1747.ep12492217.

[40] W. Boiten, S. Absalah, R. Vreeken, J. Bouwstra, J. van Smeden, Quantitative analysis of ceramides using a novel lipidomics approach with three dimensional response modelling, Biochim. Biophys. Acta (BBA) - Mol. Cell Biol. Lipids 1861 (2016) 1652–1661, https://doi.org/10.1016/j.bbalip.2016.07.004.
[41] S. Motta, M. Monti, S. Sesana, R. Caputo, S. Carelli, R. Ghidoni, Ceramide composition of the psoriatic scale, Biochim. Biophys. Acta (BBA)-Mol. Basis Dis. 1182 (1993) 147–151, https://doi.org/10.1016/0925-4439(93)90135-N.
[42] K. Vávrová, A. Kováčik, L. Opálka, Ceramides in the skin barrier, Acta Fac. Pharm. Univ. Comen. 64 (2017) 28–35, https://doi.org/10.1515/afpuc-2017-0004.
[43] I. Iwai, H. Han, L. Den Hollander, S. Svensson, L.-G. Öfverstedt, J. Anwar, J. Brewer, M. Bloksgaard, A. Laloeuf, D. Nosek, The human skin barrier is organized as stacked bilayers of fully extended ceramides with cholesterol molecules associated with the ceramide sphingoid moiety, J. Invest. Dermatol. 132 (2012) 2215–2225, https://doi.org/10.1038/jid.2012.43.
[44] E.L. Smith, N.C. Walworth, M.F. Holick, Effect of 1α,25-dihydroxyvitamin D3 on the morphologic and biochemical differentiation of cultured human epidermal keratinocytes grown in serum-free conditions, J. Invest. Dermatol. 86 (1986) 709–714, https://doi.org/10.1111/1523-1747.ep12276343.
[45] R. Gniadecki, Stimulation versus inhibition of keratinocyte growth by 1,25-dihydroxyvitamin D3: dependence on cell culture conditions, J. Invest. Dermatol. 106 (1996) 510–516, https://doi.org/10.1111/1523-1747.ep12343866.
[46] Z. Xie, S.J. Munson, N. Huang, A.A. Portale, W.L. Miller, D.D. Bikle, The mechanism of 1, 25-dihydroxyvitamin D3 autoregulation in keratinocytes, J. Biol. Chem. 277 (2002) 36987–36990, https://doi.org/10.1074/jbc.M201404200.
[47] P.R. Moll, V. Sander, A.M. Frischauf, K. Richter, Expression profiling of vitamin D treated primary human keratinocytes, J. Cell. Biochem. 100 (2007) 574–592, https://doi.org/10.1002/jcb.21061.
[48] D.D. Bikle, D. Ng, Y. Oda, K. Hanley, K. Feingold, Z. Xie, The vitamin D response element of the involucrin gene mediates its regulation by 1,25-dihydroxyvitamin D3, J. Invest. Dermatol. 119 (2002) 1109–1113, https://doi.org/10.1046/j.1523-1747.2002.19508.x.
[49] M.J. Su, D.D. Bikle, M.L. Mancianti, S. Pillai, 1,25-Dihydroxyvitamin D3 potentiates the keratinocyte response to calcium, J. Biol. Chem. 269 (1994) 14723–14729.
[50] D. Bikle, Vitamin D: production, metabolism, and mechanisms of action, Endotext [Internet], MDText. com, Inc., 2017.
[51] D.D. Bikle, Vitamin D regulated keratinocyte differentiation, J. Cell. Biochem. 92 (2004) 436–444, https://doi.org/10.1002/jcb.20095.
[52] D.D. Bikle, Y. Oda, Z. Xie, Calcium and 1,25(OH)2D: interacting drivers of epidermal differentiation, J. Steroid Biochem. Mol. Biol. 89–90 (2004) 355–360, https://doi.org/10.1016/j.jsbmb.2004.03.020.
[53] A. Slominski, T.-K. Kim, Z. Janjetovic, A. Brożyna, M. Żmijewski, H. Xu, T. Sutter, R. Tuckey, A. Jetten, D. Crossman, Differential and overlapping effects of 20,23(OH)2D3 and 1,25(OH)2D3 on gene expression in human epidermal keratinocytes: identification of AhR as an alternative receptor for 20,23(OH)2D3, Int. J. Mol. Sci. 19 (2018) 3072, https://doi.org/10.3390/ijms19103072.
[54] A.T. Slominski, T.K. Kim, J.V. Hobrath, A.S.W. Oak, E.K.Y. Tang, E.W. Tieu, W. Li, R.C. Tuckey, A.M. Jetten, Endogenously produced nonclassical vitamin D hydroxymetabolites act as "biased" agonists on VDR and inverse agonists on RORalpha and RORgamma, J. Steroid Biochem. Mol. Biol. 173 (2017) 42–56, https://doi.org/10.1016/j.jsbmb.2016.09.024.
[55] A.T. Slominski, T.-K. Kim, H.Z. Shehabi, I. Semak, E.K.Y. Tang, M.N. Nguyen, H.A.E. Benson, E. Korik, Z. Janjetovic, J. Chen, C.R. Yates, A. Postlethwaite, W. Li, R.C. Tuckey, In vivo evidence for a novel pathway of vitamin D_3 metabolism initiated by P450scc and modified by CYP27B1, FASEB J. 26 (2012) 3901–3915, https://doi.org/10.1096/fj.12-208975.
[56] A.T. Slominski, W. Li, T.-K. Kim, I. Semak, J. Wang, J.K. Zjawiony, R.C. Tuckey, Novel activities of CYP11A1 and their potential physiological significance, J. Steroid Biochem. Mol. Biol. 151 (2015) 25–37, https://doi.org/10.1016/j.jsbmb.2014.11.010.
[57] A.T. Slominski, T.-K. Kim, W. Li, A. Postlethwaite, E.W. Tieu, E.K.Y. Tang, R.C. Tuckey, Detection of novel CYP11A1-derived secosteroids in the human epidermis and serum and pig adrenal gland, Sci. Rep. 5 (2015) 14875, https://doi.org/10.1038/srep14875.
[58] G. Bakdash, L.P. Schneider, T.M. van Capel, M.L. Kapsenberg, M.B. Teunissen, E.C. de Jong, Intradermal application of vitamin D3 increases migration of CD14+ dermal dendritic cells and promotes the development of Foxp3+ regulatory T cells, Hum. Vaccine Immunother. 9 (2013) 250–258, https://doi.org/10.4161/hv.22918.
[59] A.M.G. van der Aar, D.S. Sibiryak, G. Bakdash, T.M.M. van Capel, H.P.M. van der Kleij, D.-J.E. Opstelten, M.B.M. Teunissen, M.L. Kapsenberg, E.C. de Jong, Vitamin D3 targets epidermal and dermal dendritic cells for induction of distinct regulatory T cells, J. Allergy Clin. Immunol. 127 (2011), https://doi.org/10.1016/j.jaci.2011.01.068 1532–1540.e1537.
[60] T. Akiyama, F. Niyonsaba, C. Kiatsurayanon, T. Nguyen, H. Ushio, T. Fujimura, T. Ueno, K. Okumura, H. Ogawa, S. Ikeda, The human cathelicidin LL-37 host defense peptide upregulates tight junction-related proteins and increases human epidermal keratinocyte barrier function, J. Innate Immun. 6 (2014) 739–753, https://doi.org/10.1159/000362789.
[61] I.J. Kosten, S.W. Spiekstra, T.D. de Gruijl, S. Gibbs, MUTZ-3 derived Langerhans cells in human skin equivalents show differential migration and phenotypic plasticity after allergen or irritant exposure, Toxicol. Appl. Pharmacol. 287 (2015) 35–42, https://doi.org/10.1016/j.taap.2015.05.017.
[62] S.E.L. Vidal, K.A. Tamamoto, H. Nguyen, R.D. Abbott, D.M. Cairns, D.L. Kaplan, 3D biomaterial matrix to support long term, full thickness, immuno-competent human skin equivalents with nervous system components, Biomaterials (2018), https://doi.org/10.1016/j.biomaterials.2018.04.044 In press.